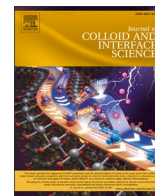




Contents lists available at ScienceDirect

## Journal of Colloid And Interface Science

journal homepage: [www.elsevier.com/locate/jcis](http://www.elsevier.com/locate/jcis)

Regular Article

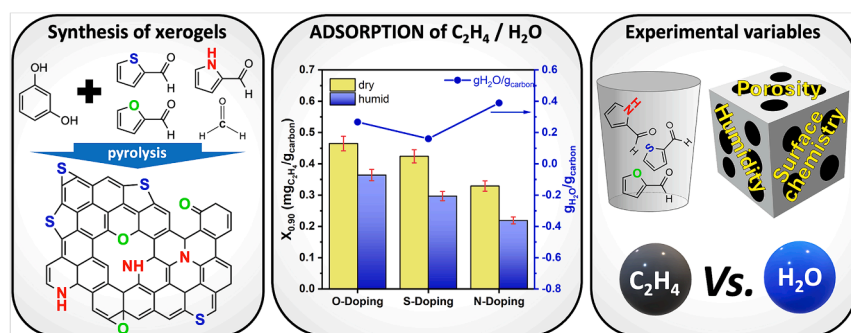
## The dynamic ethylene adsorption on carbon xerogels as a three-way game between porosity, surface chemistry and humidity

Lorena T. Pérez-Poyatos, Sergio Morales-Torres<sup>\*</sup>, Luisa M. Pastrana-Martínez, Francisco J. Maldonado-Hódar

NanoTech – Nanomaterials and Sustainable Chemical Technologies, Department of Inorganic Chemistry, Faculty of Sciences, University of Granada, Avda. Fuente Nueva s/n, ES18071 Granada, Spain



## GRAPHICAL ABSTRACT



## ARTICLE INFO

## Keywords:

Carbon xerogels  
Surface chemistry  
Porosity  
Hydrophobicity  
Dynamic adsorption  
Ethylene

## ABSTRACT

Novel carbon xerogels doped with heteroatoms (O, N, S) were prepared by sol–gel polymerization of resorcinol with heterocyclic aldehydes containing them. All doped materials presented higher O-contents than the reference material prepared with formaldehyde, and significant S- or N-loadings in the corresponding samples. Carbon xerogels were micro-mesoporous and N-doping favoured the formation of mesopores. Their efficiency in the dynamic ethylene adsorption is presented as an interplay between porosity, surface chemistry and humidity. The surface hydrophilicity was also studied by water adsorption assays, a quick adsorption being favoured in microporous samples with hydrophilic O-groups. Breakthrough curves for ethylene adsorption were recorded in both dry and humid conditions and analysed according to the mass transference zone (MTZ). The material behaviour was correlated with the physicochemical properties, elucidating the mechanism of the simultaneous water/ethylene adsorption. The adsorption capacity depended linearly on the microporous characteristics of samples; however, MTZ parameters (efficiency of the column) varied linearly with the electronegativity of the dopant element. Both doping and humidity in the stream hindered the ethylene adsorption kinetic and capacity (up to 33% for N-doped material under humidity compared to undoped-material under dry conditions), due to reduced adsorbate-adsorbent interactions and the accessibility into narrow pores.

<sup>\*</sup> Corresponding author.

E-mail address: [semoto@ugr.es](mailto:semoto@ugr.es) (S. Morales-Torres).

<https://doi.org/10.1016/j.jcis.2024.08.044>

Received 6 June 2024; Received in revised form 27 July 2024; Accepted 7 August 2024

Available online 10 August 2024

0021-9797/© 2024 The Author(s). Published by Elsevier Inc. This is an open access article under the CC BY-NC-ND license (<http://creativecommons.org/licenses/by-nc-nd/4.0/>).

## 1. Introduction

In order to make fruit and vegetables available outside harvesting season, it is necessary to handle and preserve them properly. Among them, the management of the so-called climacteric products (e.g., apples, pears, kiwis, avocados, tomatoes, etc.) should be carefully controlled because the maturation of the fruits continues once harvested, in contrast to non-climacteric products [1]. This process is carried out with the natural release of ethylene (C<sub>2</sub>H<sub>4</sub>), among other gases, from the stored fruits. Ethylene plays an important role as a hormone for ripening, stimulating the respiration and the transformation of some organic compounds (sugars), responsible for changes in colour and flavour. Even at very low concentrations (0.1 µL/L), ethylene may cause overripe, quick deterioration and senescence, shortening the products' shelf lives and consequently, leading to huge economic losses for the agricultural sector [2,3].

For this reason, it is critical to control transportation and storage conditions. Reducing temperature and limiting oxygen availability are traditional measures taken to slow down the ripening process. Thus, storage and transportation are carried out in cold chambers under controlled atmospheres (low or ultralow oxygen content, high humidity and CO<sub>2</sub> levels) to preserve fruit quality. On the other hand, ethylene concentration should be kept as low as possible using different approaches. The first option is the use of chemical inhibitors which block the production centres (i.e., 1-methylcyclopropene – 1-MCP), or avoid the ethylene release by coating fruits with waxes [4]. Alternatively, the ethylene formed may be removed or transformed into inactive molecules. New packaging systems have been developed for this purpose, such as permeable bags filled with adsorbents or strong oxidants that are included in the packaging. In particular, potassium permanganate (KMnO<sub>4</sub>) was used as ethylene scavenger, to oxidize it to CO<sub>2</sub> and H<sub>2</sub>O to a certain extent [5]. Ozone was also proposed as alternative oxidant [3]. However, both chemical methods have drawbacks associated to the limited efficiency for ethylene removal and the toxicity of the compounds used, which could entail some risks for food safety. Therefore, the development of novel, non-hazardous and sustainable alternatives for ethylene removal is of great interest for the agro-food industry. The ethylene removal by specific adsorbents is currently emerging as one of the most promising and economically competitive technologies [6,7]. Some of the materials commonly used include zeolites, silica, clays or carbon materials [6]. However, some studies revealed that carbon-based materials possess a higher structural and chemical stability, lower cost and better hydrophobicity than the rest of adsorbents, which has turned them into convenient ethylene adsorbent materials [8–10].

The adsorptive capacity of carbon materials depends on the combination of factors, such as textural properties and surface chemistry, so the ideal scenario would be to develop materials with tuneable physicochemical properties. Carbon xerogels have emerged as perfect candidates for this purpose, because both aspects can be controlled by fitting the synthesis process [11]. The synthesis of these materials was developed by Pekala *et al.* in the early 1990 s [12] and it is a two-step reaction method involving the hydrolysis and condensation of the precursors. The first works in this line were based on the aqueous (W) polymerization of resorcinol (R) and formaldehyde (F) catalysed (C) by weak bases (Na<sub>2</sub>CO<sub>3</sub>), highlighting that many variables must be carefully adjusted, as they greatly affect the properties of the final material. The wide range of variables, such as the resorcinol/formaldehyde ratio, pH of the solution, drying process or temperature and duration of the carbonization step, while increasing the difficulty of reproducing the samples, should be considered as a powerful tool to adjust the properties of the synthesized material to the specific requirements of an application. On this premise, the synthesis method has been extensively modified to adjust the porosity, surface chemistry, mechanical properties or micro- or macro-structure of carbon gels [13]. One of the approaches to adjust the chemical surface of the xerogels is based on the use of different cross-linker monomers, such as melamine [14], phenol

[15], furfural [16], phloroglucinol [17], etc., achieving carbon materials doped with different heteroatoms in their structure. The introduction of these heteroatoms generates new functional groups and active centres with different electronegativity on the supports, thus modifying surface affinity of the carbon material for specific adsorbates [18–21], such as methane [13], toluene [22], acetone [22,23], or ethylene [24], as VOC examples.

Based on the commented versatility of the sol–gel procedure to tailor the characteristics of carbon gels, we synthesized carbon gels doped with different heteroatoms (i.e., O, S and N) using heterocyclic aldehydes containing these elements as carbon precursors. These novel carbon xerogels with a tailored microsphere structure and specific composition were synthesized to elucidate the role of porosity and surface chemistry when developing efficient and selective ethylene adsorbents. The physicochemical properties, including hydrophobicity, were analysed using complementary characterization techniques and related to the performance of the samples in the elimination of ethylene from gaseous streams by adsorption under different conditions (mainly, in the presence or absence of humidity). To the best of our knowledge, this is the first study extensively dealing with the influence of the chemical surface and porosity of carbon xerogels and the presence of moisture on the stream, on ethylene removal by adsorption in dynamic conditions.

## 2. Materials and methods

### 2.1. Chemicals

*n*-heptane (C<sub>7</sub>H<sub>16</sub>, 99.8 %, VWR Chemicals), Span® 80 (C<sub>26</sub>H<sub>50</sub>O<sub>7</sub>, >60 %, Sigma Aldrich), methanol (CH<sub>3</sub>OH, >99.9 %, VWR Chemicals), resorcinol (C<sub>6</sub>H<sub>6</sub>O<sub>2</sub>, 99 %, Alfa Aesar), formaldehyde (CH<sub>2</sub>O, 37 %, Sigma Aldrich), thiophene-2-carboxaldehyde (C<sub>5</sub>H<sub>4</sub>OS, 98 %, Thermo Scientific), pyrrole-2-carboxaldehyde (C<sub>5</sub>H<sub>5</sub>NO, 98 %, Apollo Scientific), furfural (C<sub>5</sub>H<sub>4</sub>O<sub>2</sub>, 98 %, Merck), hydrochloric acid (HCl, 37 %, Labkem), acetone (C<sub>3</sub>H<sub>6</sub>O, >99 %, VWR Chemicals) and C<sub>2</sub>H<sub>4</sub>/He cylinder (1000 ppmv or 0.1 % C<sub>2</sub>H<sub>4</sub> in He, Air Liquide).

### 2.2. Synthesis of heteroatom-doped carbon xerogels

Samples were prepared in a stirred batch reactor consisting of a three-neck round-bottom flask equipped with a reflux, mechanical stirring and temperature controller. For the synthesis of the reference RF organic gel, 450 mL of *n*-heptane as reaction media, 11 mL of Span® 80 (a non-ionic surfactant) and a fitted Milli-Q aqueous solution of R, were heated up to 75 °C under stirring and reflux. Then, the appropriate amount of F solution was dropped on the preheated solution. To prepare organic doped gels, heteroatoms were introduced directly in the chemical polymeric network by replacing F with the corresponding aldehyde, namely thiophene-2-carboxaldehyde to generate S-functionalities, pyrrole-2-carboxaldehyde for N-functionalities, and furfural to increase the O-content, which were previously dissolved in methanol. All recipes maintain a R/aldehyde molar ratio of 1/2 and a R/W molar ratio of 1/8. Finally, 4 mL of HCl were added drop by drop to the suspension, aging the polymer for 24 h to guarantee complete condensation. Afterward, the organic gels were filtered and washed with abundant acetone to remove rest of solvents and unreacted products and stored in acetone suspension for 24 h, renewing acetone after each 8 h. This allows the exchange of solvents by filling the pores with acetone, which considerably reduces the shrinkage of the porosity during the drying process [25,26]. After solvent exchange, samples are recovered by filtering, dried overnight at 80 °C to completely evaporate the acetone, and stored in a desiccator to prevent humidity adsorption. The gels obtained were later carbonized in an oven under N<sub>2</sub> atmosphere at 800 °C with a soak time of 1 h and a heating rate of 3 °C/min. This carbonization temperature was chosen to provide high thermal, mechanical and structural stability to the final products. In general, the pyrolysis of organic gels is complete at around 700 °C [12,27].

The samples were labelled as A-XG, where “XG” denotes xerogel character (subcritical drying); and “A” refers to the aldehyde used during heteroatom-doping, i.e., “O” (oxygen) for furfural, “S” (sulphur) for thiophene-2-carboxaldehyde and “N” (nitrogen) for pyrrole-2-carboxaldehyde, while “C” corresponds to the reference xerogel prepared with F. Thus, the carbon xerogels C-XG (reference), S-XG, N-XG and O-XG were obtained.

### 2.3. Characterization techniques

Different complementary techniques were used to characterize the samples. The morphology of the adsorbents was studied by scanning electronic microscopy (SEM), with a high-resolution microscope Carl Zeiss SMT, model Auriga. Elemental analysis (EA) was carried out to determine the bulk chemical composition of samples using a Thermo Scientific, model Flash 2000 equipment. Thermogravimetric analysis (TGA) was performed to determine the thermal stability of the materials under air atmosphere (heating up to 800 °C and with a heating rate of 5 °C/min) using a SHIMADZU TGA-50H thermobalance. The identification of chemical groups was carried out by attenuated total reflectance coupled with Fourier Transform infrared spectroscopy (ATR-FTIR) and X-ray photoelectron spectroscopy (XPS) analysis, recorded respectively with a JASCO 6200 and a Kratos Axis Ultra-DLD to determine the nature and percentage of each chemical species on the surface. Survey and multi-region spectra were recorded at C1s, O1s, S2p and N1s photoelectron peaks and each spectral region was scanned several times to obtain good signal-to-noise ratios. The point of zero charge ( $\text{pH}_{\text{PZC}}$ ) of the samples was determined according to the procedure developed by Leon [28,29]. The content of acidic and basic surface functional groups in the carbon xerogels has been determined using Boehm titration [30]. In a typical assay, 0.10 g of sample was suspended in separate flasks containing 10 mL of HCl 0.10 M, NaOH 0.10 M,  $\text{Na}_2\text{CO}_3$  0.05 M and  $\text{NaHCO}_3$  0.10 M. The suspensions were left shaking for 48 h and then, they were filtered, and 5 mL of each solution were titrated with HCl 0.10 M or NaOH 0.10 M. The textural parameters of the samples were obtained using  $\text{N}_2$  and  $\text{CO}_2$  physical adsorption at  $-196$  °C and  $0$  °C, respectively, with a Quadrasorb SI equipment (Quantachrome). For that, the samples were outgassed for 12 h at  $110$  °C with a high vacuum of  $10^{-6}$  mbar. Brunauer, Emmett and Teller (BET) method was applied to calculate the apparent surface area ( $S_{\text{BET}}$ ) of the samples [31]; Dubinin-Radushkevich (DR) equation was used to calculate the micropore volume ( $W_0$ ) of the samples [32,33], while Stoeckli equations [34] were applied to determine the micropore surface area ( $S_{\text{micro}}$ ) and mean micropore width ( $L_0$ ). Total pore volume ( $V_{\text{T}}$ ) was considered as the volume of  $\text{N}_2$  adsorbed at a relative pressure ( $P/P_0$ ) of 0.95, which is due to the volume of micro- and mesopores according to Gurvich's rule [33,35]. The Barrett, Joyner and Halenda (BJH) method [36] and quenched solid density functional theory (QSDFT) were used to calculate the pore size distribution (PSD) [37,38]. The hydrophobicity of the carbon xerogels was determined using a gravimetric method, which estimates the amount of water vapor adsorbed into the samples at room temperature and 100 % relative humidity (RH), under static conditions until a constant weight (saturation) is achieved.

### 2.4. Ethylene adsorption assays

Ethylene adsorption was performed in dynamic conditions using glass reactors containing around 0.40 g of adsorbents sieved under 150  $\mu\text{m}$ , which form a fixed bed of  $8.0 \times 0.60$  cm. The experiments are carried out at atmospheric pressure with a total flow of  $25 \text{ cm}^3/\text{min}$  of a mixture of  $\text{N}_2/\text{O}_2/\text{C}_2\text{H}_4/\text{H}_2\text{O}$ . The fitted  $\text{C}_2\text{H}_4$  concentration in the synthetic air mixture (21 %  $\text{O}_2$ ) was 100 ppmv, while the influence of humidity was analysed by performing additional experiments in dry conditions or at 50 % RH. Adsorption experiments were carried out to obtain the breakthrough curves [39–41]. The mixture passed through the columns, and the ethylene and water exiting the outlet end of the

column were analysed using a gas chromatograph (Shimadzu GC 2010 Plus), equipped with Rt-Msievie 5A and Rt-Q-BOND columns, and a barrier discharge ionization (BID) detector.

The amount of ethylene adsorbed in the breakthrough ( $X_{0.02}$ ) and saturation points ( $X_{0.90}$ ) are compared. These points are defined as the time on stream or the eluted volume before the  $\text{C}_2\text{H}_4$  concentration measured at the outlet end of the column reached 2 % and 90 % of the initial concentration, respectively. Another important parameter is the height of the mass transfer zone ( $H_{\text{MTZ}}$ ), representing the region of the fixed bed in which adsorption is taking place, calculated following the equations (Eqs. (1)–(2):

$$H_{\text{MTZ}} = h \left( \frac{V_{0.90} - V_{0.02}}{V_{0.02} + \phi(V_{0.90} - V_{0.02})} \right) \quad (1)$$

$$\phi = \frac{\int_{V_{0.02}}^{V_{0.90}} (C_0 - C) dV}{C_0(V_{0.90} - V_{0.02})} \quad (2)$$

in which “h” is the height of the adsorption bed and “ $\phi$ ”, the fractional capacity, which evaluates the efficiency of the adsorption process. Since  $H_{\text{MTZ}}$  progressively moves along the column as the adsorbent is saturated,  $R_{\text{MTZ}}$  is defined as the rate of advance of  $H_{\text{MTZ}}$  through the fixed bed reactor, according to Eq. (3):

$$R_{\text{MTZ}} = H_{\text{MTZ}} / (t_{0.90} - t_{0.02}) \quad (3)$$

## 3. Results and discussion

### 3.1. Physicochemical characterization

The first objective was to validate the success of the synthesis process in generating stable chemical groups after carbonization at 800 °C. The bulk and surface chemical composition of the samples were obtained by EA and XPS, respectively (Table 1). The C-XG sample synthesized from the classical RF mixture was chosen as reference material. The increased O, N and S contents, according to the monomer used in each synthesis, confirm the viability of the designed procedure. Thus, the applied one-pot sol-gel method effectively generates stable chemical groups on carbon xerogels, making it an easy functionalization tool. Oxygen and nitrogen functionalities seem to be more homogeneously distributed after carbonization at 800 °C than the sulphur ones, showing a significant reduction of the surface S-content regarding the bulk concentration (i.e., 1.3 % vs. 4.3 % for  $S_{\text{XPS}}$  and  $S_{\text{EA}}$ , respectively). All materials presented slightly basic  $\text{pH}_{\text{PZC}}$  values (Table 1). Increasing the O-content typically increased the concentration of oxygen-containing surface groups, such as anhydride or ketones (carboxylic acids present a low thermal stability) with acidic character. Nevertheless, there is only a weak acidification of O-XG regarding the reference C-XG. On the contrary, N-functionalities enhanced the basic character, although again, the increase in  $\text{pH}_{\text{PZC}}$  is also moderate.

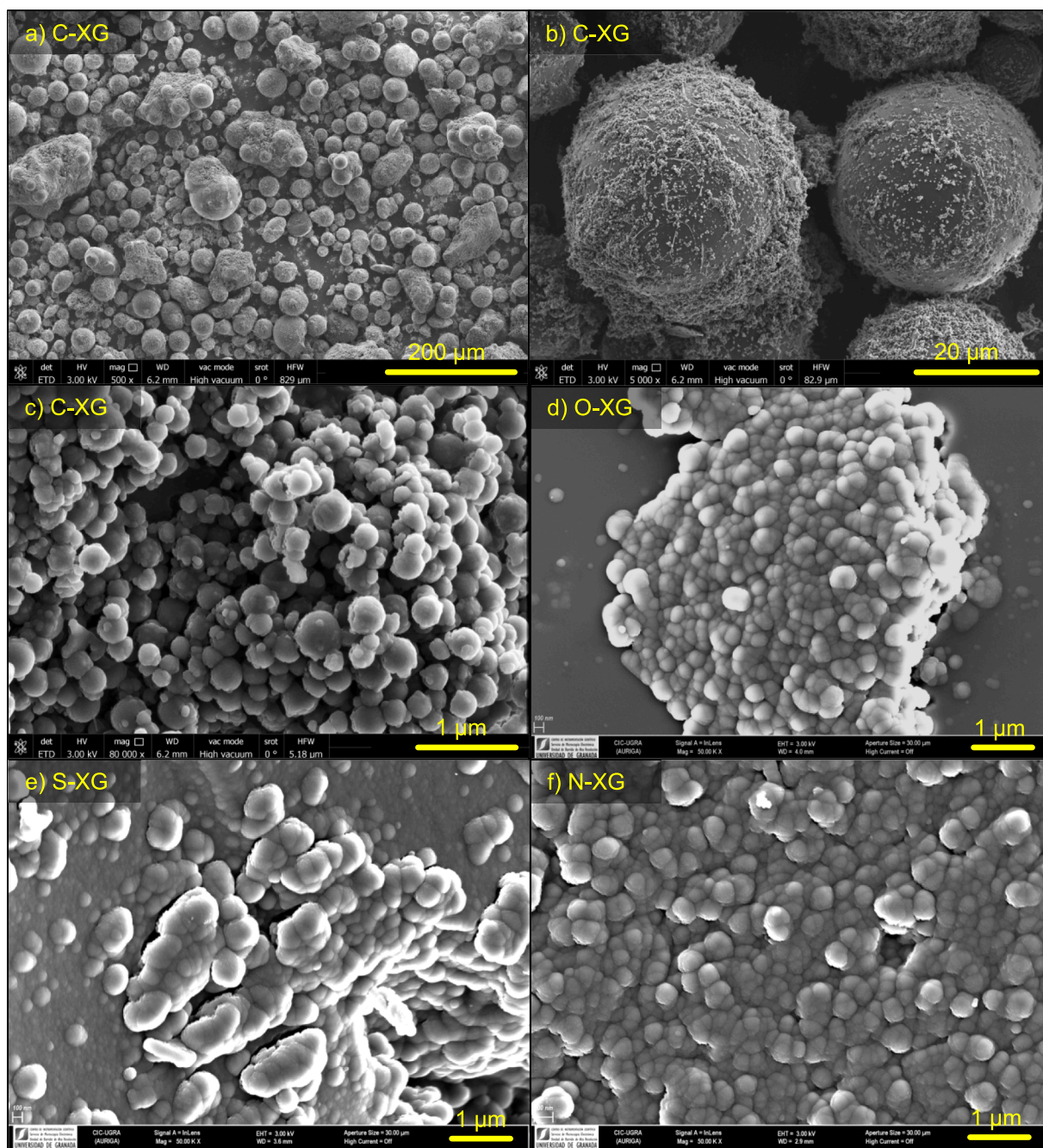
The thermal stability of the carbon xerogels under air atmosphere was studied using TGA (Fig. S1). All materials were stable below 200 °C, the mass loss (around 5 wt%) at this temperature being probably related to removal of adsorbed humidity. The combustion rate mainly increased above 400 °C. The similar profile of the TGA curves denotes the high stability of the different functional groups regardless the heteroatom element. These groups remain stable after carbonization under nitrogen atmosphere at 800 °C, thus inducing only small differences between the stability of the samples when analyzed under oxidant conditions.

The morphology of the materials was analysed by SEM. In general, the structure of the organic gels was composed of microspheres, induced by the stirring movement inside a spherical reactor and the presence of the surfactant in the starting solution. As observed in Fig. 1a, the C-XG carbon xerogel is formed by microspheres with a mean size around 20  $\mu\text{m}$ . Details of the microspheres' surface (Fig. 1b) denote that they are also formed by smaller microspheres with a mean diameter of  $\sim 0.2 \mu\text{m}$

**Table 1**Point of zero charge ( $\text{pH}_{\text{PZC}}$ ), and bulk and surface chemical composition (wt%) of heteroatom-doped carbon xerogels determined by EA and XPS, respectively.

Sample	$\text{C}_{\text{EA}}$ (%)	$\text{O}_{\text{EA}}^*$ (%)	$\text{N}_{\text{EA}}$ (%)	$\text{S}_{\text{EA}}$ (%)	$\text{H}_{\text{EA}}$ (%)	$\text{C}_{\text{XPS}}$ (%)	$\text{O}_{\text{XPS}}$ (%)	$\text{N}_{\text{XPS}}$ (%)	$\text{S}_{\text{XPS}}$ (%)	$\text{pH}_{\text{PZC}}$
C-XG	87.9	7.3	–	–	4.8	96.2	3.8	–	–	7.4
O-XG	81.7	13.2	–	–	5.1	90.5	9.5	–	–	7.1
S-XG	83.1	8.4	–	4.3	4.2	92.6	6.1	–	1.3	7.3
N-XG	79.5	9.8	6.4	–	4.3	88.7	5.8	5.5	–	7.8

\* Calculated by difference.

**Fig. 1.** SEM micrographs of (a–c) reference C-XG and (d–f) heteroatom-doped carbon xerogels: (a, b) microspheres size and (c–f) distribution of primary particles.

(Fig. 1c), typically referred to as “primary particles”. In general, heteroatom-doped carbon xerogels maintained the spherical microstructure, although with some modifications. The different aldehydes used in the synthesis modified the size and overlapping degree of the

primary particles (Fig. 1d–f), resulting in a smaller size (around 0.1  $\mu\text{m}$ ) and a larger overlapping degree, creating different opened porosity (meso- and macropore distribution) between the primary particles.

Textural properties of samples are closely related with the previously

described morphology. Thus, the PSD of samples obtained by sol-gel procedures depends on the combination of numerous processes carried out during synthesis. The polymerization step defines the shape, dimension and overlapping of primary particles forming the 3D-network, which basically define the mesoporous range. In contrast, the heat treatment conditions determine the pyrolysis degree and the release of gases, which in turn, develop the microporosity [25,26]. The shrinkage undergone during these processes is related not only with the selected drying method or carbonization conditions, but also with the mechanical properties of the samples [25,42].

The textural characterization of the samples was carried out by determining the complementary adsorption isotherms of  $N_2$  and  $CO_2$  (Fig. 2a and b). The textural parameters obtained from the analysis of these isotherms, according to the procedures described in the experimental section, are listed in Table 2. The  $N_2$  adsorption-desorption isotherms of carbon xerogels (Fig. 2a) belong to type I and IV of the IUPAC classification. In fact, only the isotherm of N-XG is mainly a type IV isotherm, characteristic of mesoporous materials. These profiles denote the hierarchical PSD of materials, combining the intrinsic microporous nature of the samples with the presence of some mesopores. At a glance, it is observed that all doped carbon xerogels present a lower porosity ( $V_T$ ) than the reference material, except in the case of N-XG. The  $N_2$  adsorption at low relative pressure ( $P/P_0$ ) is always smaller than for the reference sample, this decrease being especially notorious for N-XG, denoting a lower microporosity (Fig. 2a). Moreover, the wider neck observed in the isotherms of S-XG and mainly, O-XG samples, suggest the formation of a more heterogeneous microporosity in these samples. At  $P/P_0 > 0.4$ , the slope of the curves and the hysteresis loop denote the presence of mesopores in all cases. The hysteresis loop is in general of type H4, with exception of N-XG, that becomes type H3, both related with slit-shaped pores. As note, the slope of the isotherms progressively increased in the trend S-XG < O-XG < C-XG < N-XG, indicating

an increased mesoporosity in this sense. For the N-XG sample, the deep increase of the amount adsorbed from  $P/P_0 > 0.8$  denotes the presence of larger mesopores than in the rest of samples. Simultaneously, the H3 hysteresis cycle also implies a deeper influence of the microporous range on the condensation/evaporation of  $N_2$  [14,43]. Thus, N-XG should present a well-developed mesoporosity formed by larger mesopores, but a reduced microporosity consisting of large micropores.

The texture analysis of the samples is corroborated by determining the PSD by QSDFT and BJH methods, which are in good agreement (Fig. 2c and d). QSDFT confirms that, in general, samples are mainly microporous (Fig. 2c). It is noteworthy that the reference carbon xerogel (C-XG) presents the narrowest microporosity but also a certain contribution of mesopores with a diameter of around 3 nm. As expected, larger mesopores with a diameter around 13 nm were found for the mesoporous N-XG, in good agreement with the value of 17 nm detected by BJH method (Fig. 2d). Both methods also confirm the scarce mesoporous character of both S-XG and O-XG samples.

A deeper characterization of the microporosity was carried out by applying DR and Stoeckli (DR-S) equations to the  $N_2$  adsorption data (Table 2). As expected, heteroatom-doping reduces the micropore volume ( $W_0$ ) of the samples, but  $L_0$  values strongly increased regarding the reference material. The mesoporous volume ( $V_{meso}$ ) also decreased, with exception of N-XG. The lower porosity of the heteroatom-doped gels is also verified by a decreased surface area. In fact, when comparing  $S_{BET}$  and  $S_{micro}$  from  $N_2$  isotherm data, similar values were obtained only for C-XG. In the heteroatom-doped gels,  $S_{BET}$  is always higher than  $S_{micro}$ , and the decrease of surface by doping is larger for  $S_{micro}$  values than for  $S_{BET}$ , pointing out that the stronger transformations take place at the micropore range.

The  $CO_2$  adsorption of the samples complements the characterization of microporosity, allowing a more detailed analysis of the narrowest microporosity (diameter < 0.7 nm). Comparing the  $CO_2$  isotherms

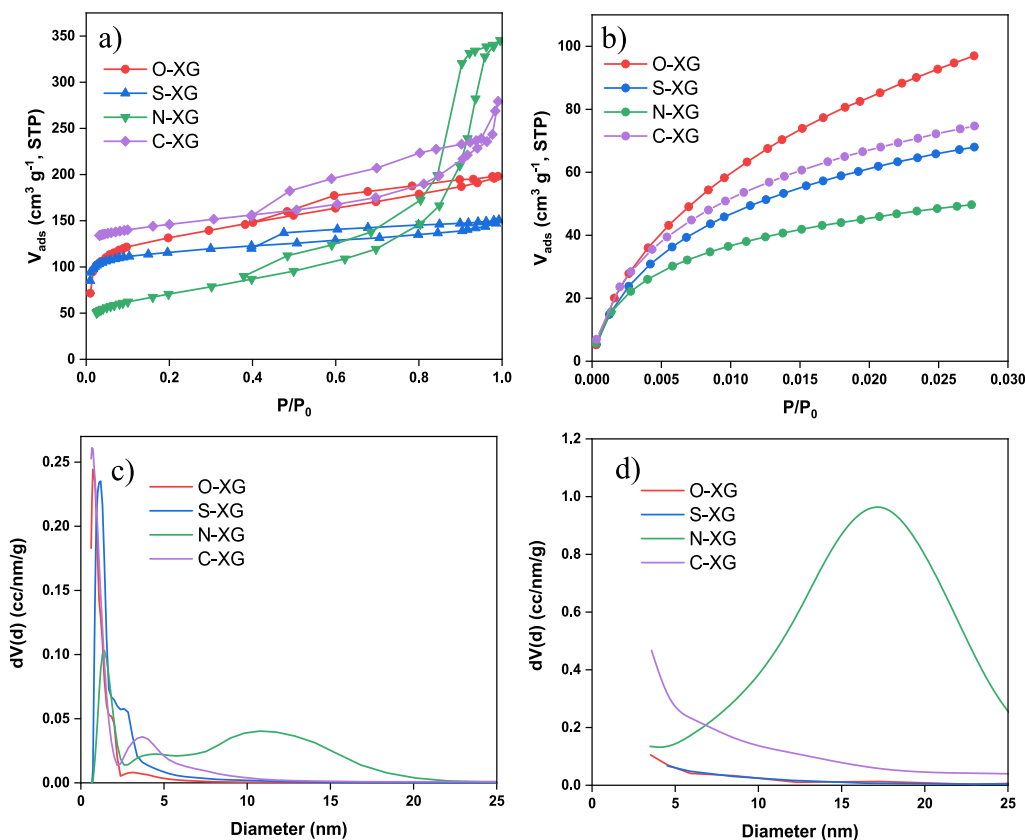


Fig. 2. Adsorption isotherms of (a)  $N_2$  and (b)  $CO_2$  for the different carbon xerogels. PSD obtained by applying (c) QSDFT and (d) BJH method to the  $N_2$  adsorption data.

Table 2

Textural parameters of the heteroatom-doped carbon xerogels.

Sample	N <sub>2</sub> adsorption						CO <sub>2</sub> adsorption			S <sub>micro</sub> CO <sub>2</sub> /S <sub>micro</sub> N <sub>2</sub>
	S <sub>BET</sub> (m <sup>2</sup> /g)	V <sub>T</sub> (cm <sup>3</sup> /g)	V <sub>meso</sub> (cm <sup>3</sup> /g)	W <sub>0</sub> (cm <sup>3</sup> /g)	L <sub>0</sub> (nm)	S <sub>micro</sub> (m <sup>2</sup> /g)	W <sub>0</sub> (cm <sup>3</sup> /g)	L <sub>0</sub> (nm)	S <sub>micro</sub> (m <sup>2</sup> /g)	
C-XG	545	0.35	0.11	0.23	0.82	555	0.26	0.57	905	1.6
O-XG	495	0.30	0.07	0.21	1.26	288	0.37	0.60	1108	3.8
S-XG	444	0.22	0.03	0.18	1.70	223	0.25	0.66	823	3.7
N-XG	254	0.44	0.30	0.11	1.86	115	0.16	0.61	630	5.5

S<sub>BET</sub> = BET surface area; V<sub>T</sub> = total pore volume; V<sub>meso</sub> = mesoporous volume; W<sub>0</sub> = micropore volume; L<sub>0</sub> = mean micropore width; S<sub>micro</sub> = microporous surface area; S<sub>micro</sub> CO<sub>2</sub>/N<sub>2</sub> = microporous surface area ratio obtained from CO<sub>2</sub> and N<sub>2</sub> isotherm data.

(Fig. 2b), it is observed that the narrow microporosity is favoured in O-XG, and deeply reduced in the mesoporous N-XG carbon xerogel, regarding the reference material. Increasing the oxygen content in the 3D-structure of the raw organic xerogel by using furfural, a higher CO<sub>x</sub> release favoured the development of narrow micropores and thereby, S<sub>micro</sub>. On the contrary, pyrrole-2-carboxaldehyde reduced the microporosity in all ranges (W<sub>CO2</sub> and W<sub>N2</sub>), and consequently, N-XG presented the smallest surface area, despite the high V<sub>meso</sub> developed. Meanwhile, thiophene-2-carboxaldehyde exhibits an intermediate behaviour; in this case, the larger reduction regarding the reference sample takes place in the mesopore range. Thus, the different monomers used during heteroatom-doping entail significant changes in the textural parameters of the samples, as previously reported [44–46]. As a general comment, both S<sub>micro</sub> and W<sub>0</sub> determined from CO<sub>2</sub> adsorption were always higher than those obtained from N<sub>2</sub> adsorption, thus denoting the N<sub>2</sub>-diffusion restriction to the narrowest microporosity. This fact is clearly pointed out when comparing the S<sub>micro</sub>(CO<sub>2</sub>)/S<sub>micro</sub>(N<sub>2</sub>) ratio, which strongly increased after doping, more markedly in the case of the mesoporous N-doped sample (Table 2). As note, mesoporous materials present the strongest diffusion problems to the entrance of the microporosity, despite the large micropore size (L<sub>0</sub>).

The adsorptive behaviour of samples will be influenced by both textural and chemical characteristics. Thus, together with the extent and accessibility to the surface (PSD), the distribution and concentration of chemical groups on these surfaces determine the strength of the interactions with a specific adsorbate. The main surface functionalities incorporated in the samples was studied by ATR-FTIR (Fig. 3). In general, the intensity of the FTIR bands in the doped samples increases regarding the reference material. These bands were assigned according to the literature [47–49]. Specifically, the broad band in the region between 3700–3100 cm<sup>-1</sup> observed in all samples was assigned to —OH

stretching vibrations, also overlapping in the N-doped sample with the vibration of terminal —NH groups. In the region of 2800–2900 cm<sup>-1</sup>, two peaks at 2850 cm<sup>-1</sup> and 2920 cm<sup>-1</sup> were assigned to symmetric and asymmetric CH<sub>2</sub> aliphatic stretching vibrations. These bands are significantly more intense for S-XG, denoting the presence of aliphatic structures and, probably, a smaller aromatic character. However, no signal for the —SH stretching peak is observed at 2570 cm<sup>-1</sup> for this sample. In the region of ~1700 cm<sup>-1</sup>, the oxygenated surface groups are detected, the peak at ~1740 cm<sup>-1</sup> being assigned to the carbonyl C=O stretching of carboxylic, anhydrides or lactonic structures [49]. It is noteworthy the different distribution of oxygenated surface groups in the samples, since this band is not observed in O-XG and N-XG samples, in which the band at ~1600 cm<sup>-1</sup> is reinforced. The signals in the region 1500–1600 cm<sup>-1</sup> are associated with conjugated C=C bonds. The C=C vibration in aromatic rings was assigned at ~1590 cm<sup>-1</sup>, while C=C in condensed aromatic rings was designated at ~1550 cm<sup>-1</sup>, the latter favoured in the case of N-XG. In the 1000–1300 cm<sup>-1</sup> region, multiple and overlapped weak bands due to C—O (phenols, alcohols or ether bridges between rings) and C—N bonds at ~1250 cm<sup>-1</sup> or N—CH<sub>3</sub> bonds at ~1372 cm<sup>-1</sup> were also previously reported [48].

High resolution XPS spectra of the C1s (Fig. 4a, b) and O1s (Fig. 4c–f) regions were analysed, together with the signals of the corresponding S- or N-doping element, i.e., S2p (Fig. 4g) or N1s regions (Fig. 4h), respectively. The nature and concentration of chemical species from deconvolution of each specific spectral region were assigned according to the literature [39,50], and are summarized in Table S1 of the Supplementary Material. The deconvolution of the C1s region (Fig. 4a and b) was carried out using four components assigned as follows: C—C (284.6 eV); C—O (~285 eV); C=O (~286 eV) and O—C=O (~289 eV). As observed, all heteroatom-doped carbon xerogels showed an increased surface O-content (Table 1). The C1s profile for S-XG was comparable to that of the reference sample, probably associated with a low S-content in surface. On contrast, the C1s profile for N-XG is significantly wider and shows a slower decay, which confirms the C—N functionalization. The peaks corresponding to C—O bonds and C—N or C—S bonds overlap between them, leading to larger tails on the corresponding spectra.

Two components were normally used to fit the deconvolution of the high-resolution O1s spectra, of the carbon materials (Fig. 4c–f), assigned as C=O and C—O bonds at ~531.5 eV and ~533.0 eV, respectively [39]. In the case of heteroatom-doped carbon xerogels, the O1s profile significantly enlarged, indicating the formation of additional surface groups, in which oxygen is linked to these heteroatoms. Thus, new components at ~532.3 eV and ~534.6 eV, associated with S—O and N—O bonds [45,50], were included to fit the deconvolution of O1s region for S-XG and N-XG, respectively. The nature of N- and S-containing groups was more specifically determined by analysing the S2p or N1s spectral regions. In this context, the deconvolution of the S2p region, with a typical peak splitting of 1.2 eV between S2p<sub>3/2</sub> and S2p<sub>1/2</sub>, for S-XG is shown in Fig. 4g. The main contribution observed at ~163.9 eV corresponds to C—S—C structures, such as those existing in the raw thiophene-2-carboxaldehyde, corroborating its incorporation in the 3D-network structure. In addition, other smaller components were assigned

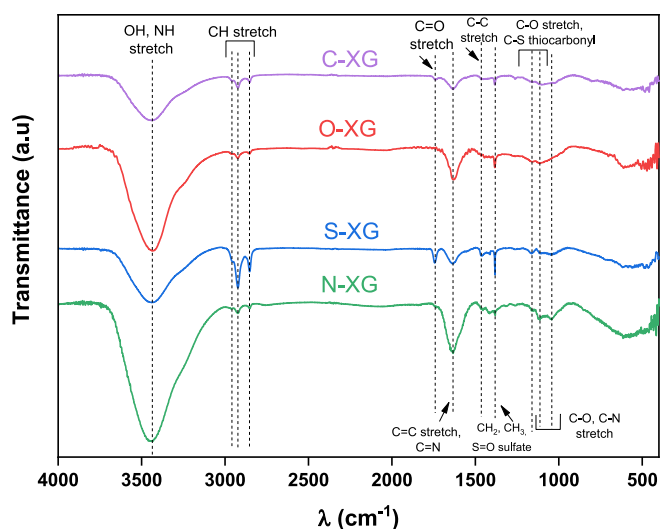


Fig. 3. ATR-FTIR spectra of the reference and heteroatom-doped carbon xerogels.

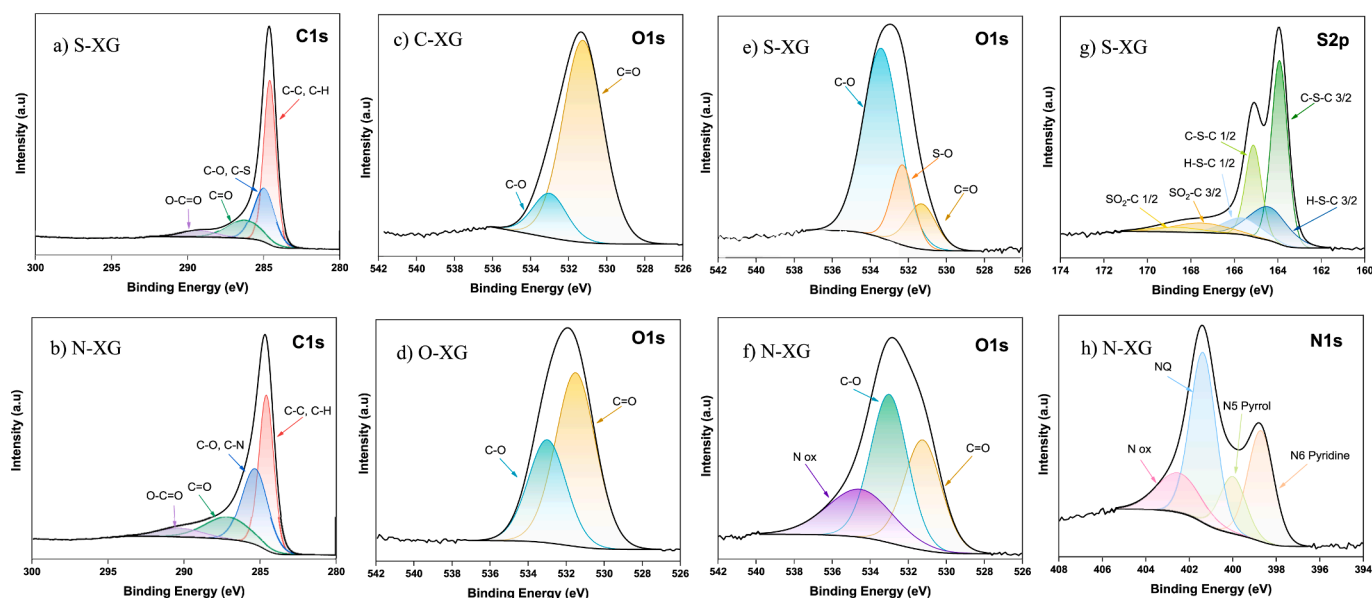


Fig. 4. XPS spectra and deconvolution of the (a, b) C1s, (c-f) O1s, (g) S2p and (h) N1s regions for selected carbon xerogels.

at  $\sim 164.4$  eV and  $\sim 167.5$  eV, associated to H—S—C and oxidized sulphur moieties (e.g., sulfones, sulfonates or sulphates), respectively [44,45]. The deconvolution of the N1s region for N-XG (Fig. 4h) shows four components associated to pyridinic N6 ( $\sim 398.7$  eV), pyrrolic N5 ( $\sim 400.0$  eV), quaternary N ( $\sim 401.4$  eV) and oxidized nitrogen species (N ox) ( $\sim 402.5$  eV) [50]. The main component was the one due to quaternary nitrogen groups, which should also justify the incorporation of the raw chemical compound to the N-XG structure during the synthesis.

The concentration of basic and acidic surface groups created in the different carbon xerogels was determined by Boehm titration, and the results are shown in Table 3. According to this procedure, titration with HCl or NaOH was used to determine the total basic and acid functionalities, respectively. The distribution of acid sites is analysed, by comparison, with the results obtained by titration with  $\text{Na}_2\text{CO}_3$ , which determines carboxylic acid groups and lactones, regarding  $\text{NaHCO}_3$ , only able to titrate carboxylic acid groups. These results are in good agreement with the evolution of the  $\text{pH}_{\text{PZC}}$  values (Table 1), as well as with the variation of the chemical composition determined by both XPS and EA. Thus, a higher oxygen content in all doped xerogels compared to the reference C-XG sample, induces an increased acidity from 1.8 to around 3.0 mmol/g, slowly increasing as follows: C-XG < N-XG < S-XG < O-XG. Similarly,  $\text{pH}_{\text{PZC}}$  values pointed out the most basic character of N-XG, which is also confirmed by the highest concentration of basic groups determined by HCl titration, i.e., a value of 5.2 mmol/g.

### 3.2. Adsorptive behaviour of water under static assays

Considering the high RH (90–99 %) used in the storage cameras of climacteric fruits, the hydrophobicity of the adsorbents is one of the

Table 3

Quantification of acidic and basic functional groups in the carbon xerogels with Boehm titration.

Concentration of functional groups (mmol/g)	C-XG	O-XG	S-XG	N-XG
Basic surface groups	2.5	2.2	2.7	5.2
Carboxylic groups	0.4	0.6	0.8	0.5
Lactones	0.1	0.5	0.2	0.6
Phenols	1.3	1.9	1.8	1.6
Total acidic surface groups	1.8	3.0	2.8	2.7

most determining properties. In this context, water adsorption was measured gravimetrically over time as a first attempt to estimate the interactions between the carbon surface and the adsorbates. Experiments were carried out up to constant weight (saturation) in static air, at room temperature and 100 % RH. Results are compiled in Table 4 and Fig. 5. It is well known that water adsorption is related with both microporosity and surface chemistry, namely with the presence of hydrophilic surface groups [51]. Although different mechanisms of water vapor adsorption were proposed, in general it is accepted that water vapor adsorption is initiated on the surface functional groups by hydrogen bonding. Then, with an increase in the amount of water adsorbed, they are forming molecular clusters that coalesce, favoured by capillarity occurred inside the pores, and condense filling the available pore volume. Thus, the concentration and nature of the surface groups determine water adsorption–desorption processes.

The interaction of RF carbon aerogels with water was recently studied by Mónica Kéri *et al.* [52], who prepared two samples with different microporosity (0.35 vs. 0.25  $\text{cm}^3/\text{g}$ ) and mesoporosity (1.31 vs. 0.84  $\text{cm}^3/\text{g}$ ), but with a similar total water uptake (0.16  $\text{cm}^3/\text{g}$ ) at 100 % RH, as deduced from water adsorption isotherms at 25 °C. This value is significantly smaller than the pore volume deduced by  $\text{N}_2$  adsorption even for the least porous sample. Additional experiments followed by nuclear magnetic resonance (NMR) cryoporometry after exposing powdered samples to different amounts of water, determined the amount of water adsorbed in each case, which increased up to 4.8 and 1.2  $\text{cm}^3/\text{g}$ , respectively. Results showed that water is adsorbed on the hydrophilic functional groups, forming water clusters and filling the micropores, according to the mechanism generally described, although the wetting of the mesopores differs.

The growing clusters of adsorbed water in mesopores lead to the formation of spherical water drops which are non-homogeneously distributed. Pore filling is sequential and progressive, wetting is plug-like, i.e., only once a pore is filled the wetting passes to the next pore through the interconnected pore structure, increasing the amount of water adsorbed up to the complete pore filling at saturation. The

Table 4

Amount of water adsorbed by the carbon xerogels in static conditions.

Water adsorbed	C-XG	O-XG	S-XG	N-XG
Q, g (water)/g (sample)	0.473	0.267	0.160	0.389
mg (water)/ $S_{\text{BET}}$	0.862	0.545	0.360	1.535

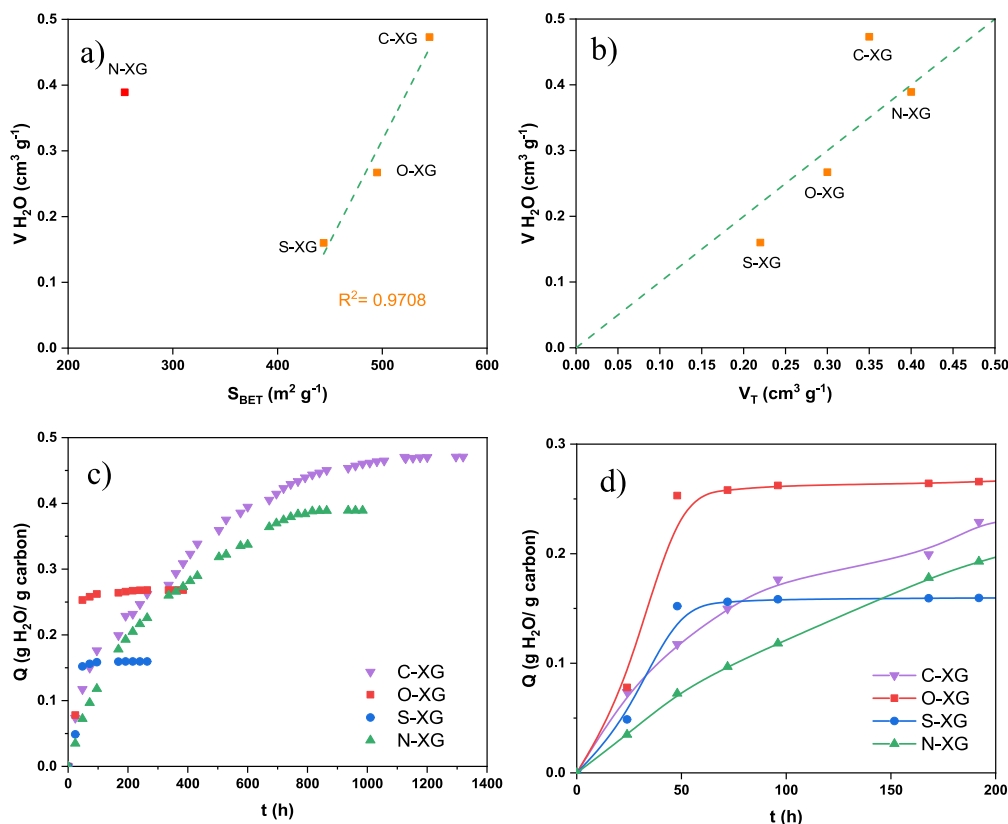


Fig. 5. Relationship between water adsorption capacity and (a) the BET surface area or (b) the total pore volume, in static conditions. (c) Adsorption kinetic curves at long times and (d) details of adsorption during the first stages in static conditions.

mechanism of water diffusion depends on the degree of wetting. When initially water forms clusters around the hydrophilic functional groups in the empty meso- and macropores, or even when the mesopores are partially filled, the porosity is still sufficient for diffusion to take place mainly in the vapour phase. However, the micropores are easily filled and, in this case, diffusion takes place in liquid phase from and into the free mesopores that are connected with these micropores. The mesopores are then filled and finally, even the macropores through the interconnected pore structure. When filling macroporosity, the volume of water adsorbed overpasses the pore volume determined from the corresponding N<sub>2</sub> adsorption-desorption isotherms, because macropores are not quantified by this technique.

Comparing the adsorptive behaviour of these carbon xerogels with those reported by Mónica Kéri *et al.* [52], a water adsorption capacity higher than 0.16 cm<sup>3</sup>/g (Table 4, Fig. 5) is observed, although our samples exhibit a lower porosity (Table 2). Thus, it can be concluded that the introduction of heteroatoms could effectively enhance the hydrophilic character of surfaces. To explore the relationship between textural and chemical aspects, the amount of adsorbed water was plotted against the BET surface area of the samples (Fig. 5a). In general, water adsorption increased linearly with  $S_{BET}$  (Fig. 5a), denoting the predominant factor of the textural properties. The highest water adsorption capacity observed in the N-XG sample (Fig. 5a) might be justified by the establishment of hydrogen bonding between N-containing surface groups and water molecules, which is also pointed out by the highest water adsorption capacity normalized per surface area unit (Table 4). Nevertheless, this type of interactions should also be accessible to oxygenated surface groups, but despite the high hydrophilicity and content of these groups, the amount of water adsorbed per square meter for O-XG is significantly lower than for N-XG, and even lower than for C-XG. In fact, the largest water adsorption takes place in the undoped sample (Table 4).

Therefore, considering these results, the overall texture was considered, instead of only the surface area values. When comparing the volume of water adsorbed directly with the total pore volume determined by N<sub>2</sub> adsorption at  $P/P_0 = 0.95$  (Fig. 5b), a linear relationship between both parameters is obtained, the volume of water adsorbed at saturation entirely matching the  $V_T$ , although with values slightly below. As noted, the undoped C-XG sample presents now an adsorbed volume that exceeds the  $V_T$ . This fact could be related with its different PSD, in agreement with the SEM analysis (Fig. 1), which showed a more opened structure between the primary particle network, probably forming a large network of macropores contributing to water adsorption [52]. The good linearity of results suggested that the total water adsorption capacity is independent of surface chemistry at saturation in static conditions, porosity being completely filled by adsorbed water, with  $V_T$  determined by N<sub>2</sub> adsorption being a good basis of comparison between different samples.

However, if only the adsorption capacity at saturation is considered, the effect of surface chemistry may be masked. The combination of porosity and surface chemistry effects on water adsorption is more evident when analysing the adsorption kinetic curves (Fig. 5c and d). There is a clear difference between the samples according to their porous structure, also in agreement with the general water adsorption mechanism [51,52]. When adsorbents are mainly microporous (O-XG and S-XG), the saturation is achieved after 2 days at room temperature and 100 % RH, while mesoporous samples (C-XG and N-XG) continue adsorbing water during longer time periods. In fact, the saturation of C-XG takes place after around 45 days (Fig. 5c) but the saturation time for N-XG is shorter (around a month), despite its largest mesopore volume. Thus, once again, the presence of hydrophilic N-containing surface groups and the mesoporous character of this sample could favour a faster water adsorption rate, shortening saturation time compared to C-XG. Nevertheless, when observing in detail the adsorption kinetic curves

at low adsorption times (Fig. 5d), water adsorption of N-XG is apparently slower than the other samples, indicating a stronger diffusion restriction to the microporosity, as previously discussed on the evolution of the  $S_{\text{micro}}(\text{CO}_2)/S_{\text{micro}}(\text{N}_2)$  ratio (Table 2). These results (Fig. 5d) confirm that the quick water adsorption is strongly favoured by the combination of a high microporous surface and the highly hydrophilic oxygenated surface groups, both aspects enhancing the adsorption rate on O-XG.

### 3.3. Adsorptive behaviour of ethylene under dynamic assays

The hydrophilicity of the samples should influence their adsorptive behaviour for ethylene under dynamic experiments. The corresponding breakthrough curves obtained in air flow (25 cm<sup>3</sup>/min) containing

100 ppmv of C<sub>2</sub>H<sub>4</sub> under dry or humid (50 % RH) conditions are shown in Fig. 6a and b, respectively. The amount of ethylene adsorbed, obtained by integration of the curves at the breakthrough and saturation points ( $C/C_0 = 0.02$  and 0.90, respectively) in both dry and humid conditions, is collected in Table 5. The ethylene adsorption depends on both surface chemistry and atmosphere conditions (Fig. 6a and b), the presence of humidity and doping clearly triggering a negative effect (curves shifted to a lower time on stream). This behaviour is summarized in Fig. 6c, in which a similar decay of the adsorption capacity by humidity (Red.= ~0.12 mg/g, Table 5) is obtained regardless of the porosity or surface chemistry of the samples, as well as a progressive reduction by doping effect in this sense: C-XG>O-XG>S-XG>N-XG. Similar results were previously reported for different series of carbon materials in the adsorption of non-polar VOCs [53]. Doping with

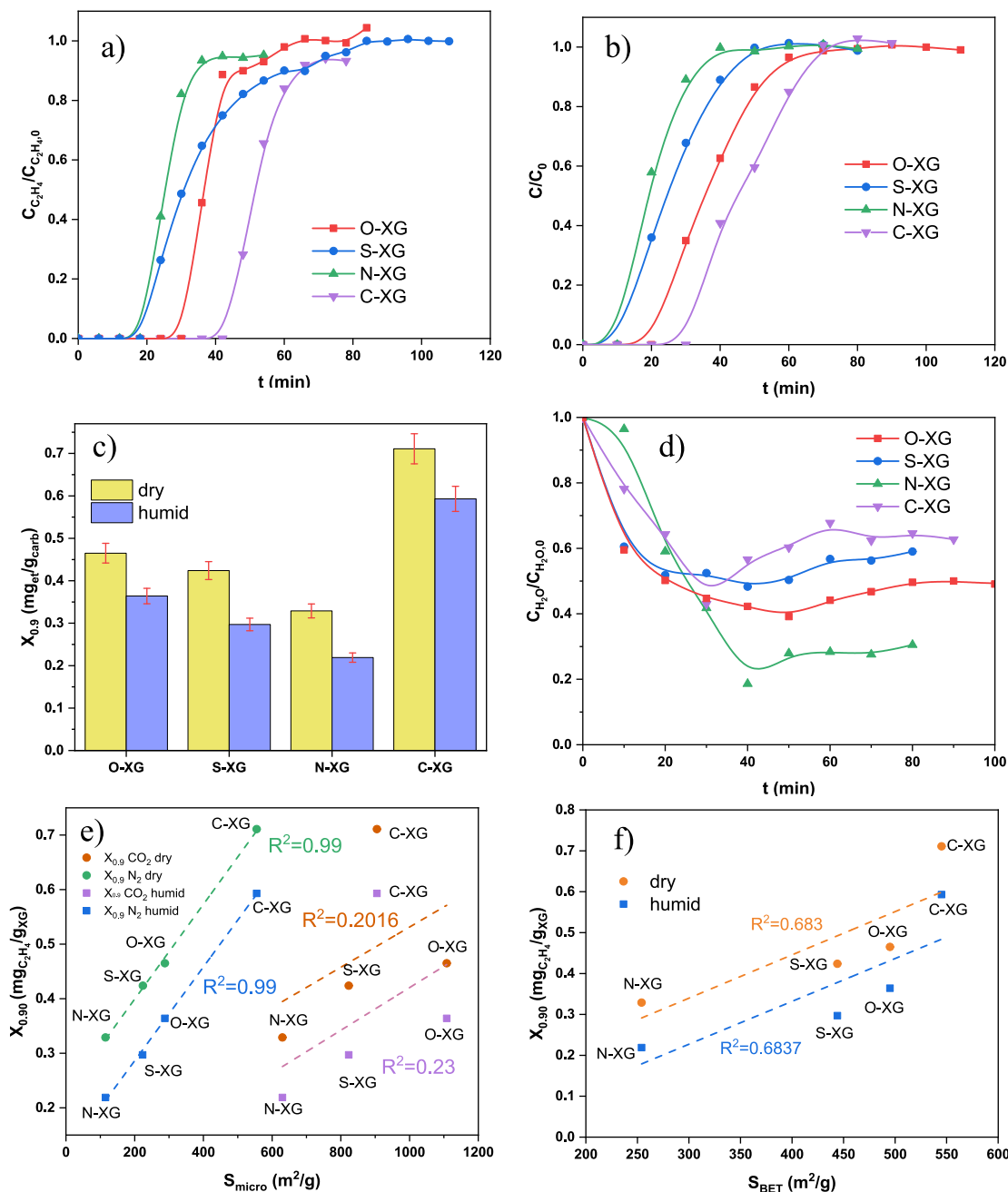


**Fig. 6.** Breakthrough curves of ethylene adsorption under dynamic assays in (a) dry and (b) humid conditions. (c) Influence of heteroatom-doping in carbon xerogels on  $X_{0.90}$ . (d) Breakthrough curves of water adsorption under dynamic assays. (f, g) Correlations between  $X_{0.90}$  and BET or microporous surface areas, respectively, in carbon xerogels in dry and humid conditions.

**Table 5**

Adsorption parameters obtained at the breakthrough and saturation points for the carbon xerogels.

Sample	$X_{0.02}$ dry ( $\text{mg}_{\text{C}_2\text{H}_4}/\text{g}_{\text{XG}}$ )	$X_{0.90}$ dry ( $\text{mg}_{\text{C}_2\text{H}_4}/\text{g}_{\text{XG}}$ )	$X_{0.02}$ humid ( $\text{mg}_{\text{C}_2\text{H}_4}/\text{g}_{\text{XG}}$ )	$X_{0.90}$ humid ( $\text{mg}_{\text{C}_2\text{H}_4}/\text{g}_{\text{XG}}$ )	Red *	$X_{0.90, \text{humid}}/S_{\text{BET}}^\dagger$	$X_{0.90, \text{humid}}/S_{\text{micro}}^\dagger$
C-XG	0.599	0.711	0.430	0.593	0.12	1.09	0.66
O-XG	0.430	0.465	0.286	0.364	0.10	0.74	0.33
S-XG	0.258	0.424	0.143	0.297	0.13	0.69	0.36
N-XG	0.258	0.329	0.143	0.219	0.12	0.86	0.35

\* Influence of the 50 % RH on the amount of  $\text{C}_2\text{H}_4$  adsorbed as:  $\text{Red} = X_{0.90, \text{dry}} - X_{0.90, \text{humid}}$ ;  $^\dagger$  Adsorption capacity of  $\text{C}_2\text{H}_4$  (in  $\mu\text{g}_{\text{C}_2\text{H}_4}/\text{g}_{\text{XG}}$ ) by unit of BET surface area or by microporous surface from  $\text{CO}_2$  isotherm data.

heteroatoms generates sites changing the polarity of surfaces according to their different electronegativity (EN) and the nature of the different surface groups that they can form. Since the ethylene molecule is non-polar, doping should produce a negative effect on the adsorbate–adsorbent interactions, reducing the adsorption capacity regarding the undoped carbon surfaces. However, according to this reasoning, the highest reduction should occur in the O-XG sample, which showed the highest surface functionalization of hydrophilic sites. Therefore, the adsorptive behaviour of each sample is due to a specific combination of porous texture and surface chemistry.

For a further correlation between the physicochemical properties and adsorptive behaviour of the materials, the total ethylene adsorption capacity ( $X_{0.90}$ ) was firstly correlated with their porous texture. Thus,  $X_{0.90}$  linearly increased with BET surface area (Fig. 6e) regardless of adsorption being performed in dry or humid conditions, the largest deviation being observed for C-XG. Although the adsorption capacity decreased in humid conditions, the relationship between both parameters is very close and parallel. This linear fitting is markedly improved when  $X_{0.90}$  is plotted against the microporous surface area ( $S_{\text{micro}}$ )

calculated by applying Stoekli's equation to  $\text{N}_2$ -adsorption data (Fig. 6f). However, the fitting was worse considering only the narrow microporosity determined by  $\text{CO}_2$  adsorption, in particular for the performance of C-XG. Therefore, the largest influence on ethylene adsorption capacity seems to be controlled by large micropores, which are accessible to  $\text{N}_2$  at  $-196^\circ\text{C}$ , with the textural properties determining the adsorption performance, in agreement with previous studies [40,54].

The presence of moisture clearly produces a negative effect on ethylene removal. The reduction in ethylene adsorption increased from 17 % for C-XG to 33 % for N-XG. However, rather than differentiating the ethylene adsorption performance according to the hydrophilicity of samples, moisture seems to homogenize the results. These different percentages are only a mathematical effect, since as mentioned above, all samples showed a similar reduction in adsorption capacity (i.e.,  $\sim 0.12$  mg/g, Table 5) and thereby, the loss as a percentage is larger for samples that adsorb less ethylene. On the contrary, under humid conditions, it is observed that: (i) the uniformity in the shape of the ethylene breakthrough curves is greater, with curves becoming more or less parallel (Fig. 6b); (ii) the adsorption capacity per area unit becomes

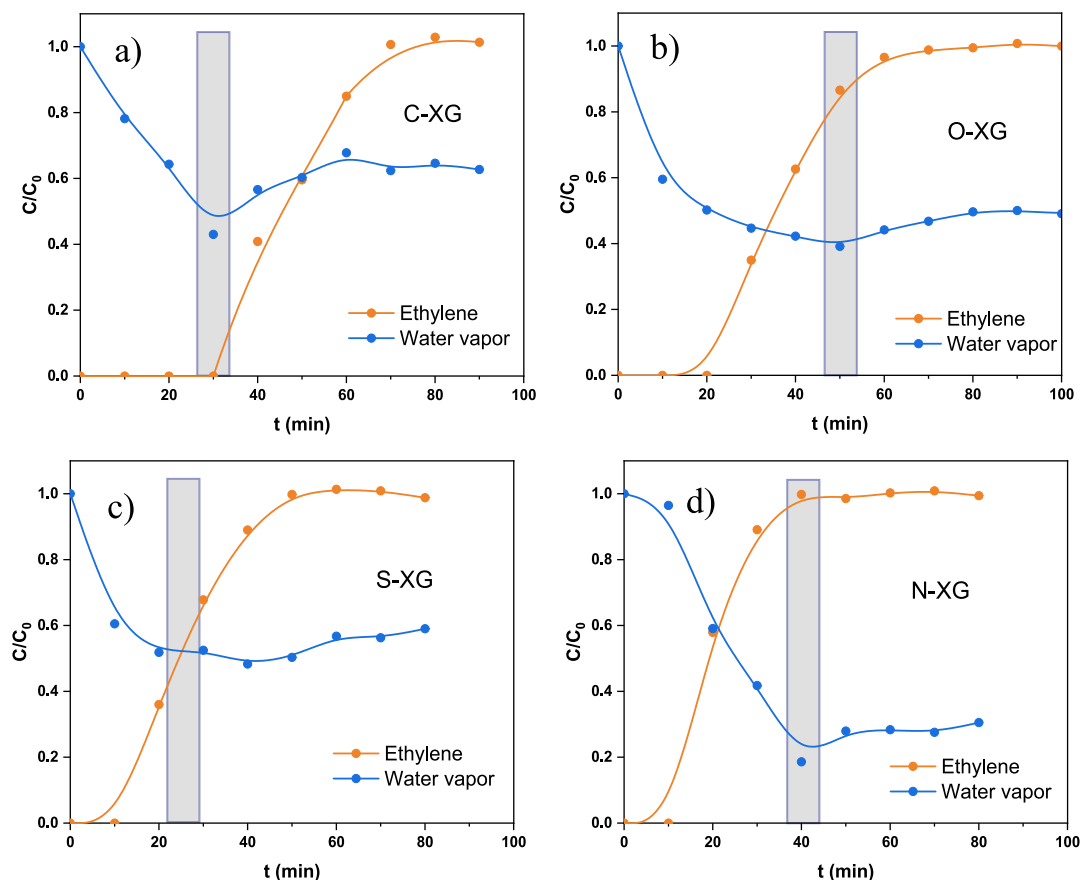


**Fig. 7.** Comparison of the profiles of ethylene and water adsorption obtained for the carbon xerogels in humid conditions (dynamic assays). (The drawn grey bar represents the time after which water concentration is stabilized).

similar for all the doped samples ( $X_{0.90}/S_{\text{micro}} \approx 0.33\text{--}0.36$ , Table 5); and (iii) the ethylene adsorption capacity decreases by a similar value in all samples, regardless of porosity or surface chemistry.

Since ethylene and water are simultaneously introduced in the feed stream of the column, the evolution of water adsorption throughout these experiments was studied deeply. The kinetics of water adsorption on the different samples are compared in Fig. 6d, while the kinetics of both water and ethylene adsorption are shown together in Fig. 7. At short times, ethylene is totally adsorbed, remaining undetected until the breakthrough point ( $t_{0.02}$ ). After that, the concentration increases until it returns to the initial value ( $t_{0.90}$ ). On the contrary, water vapour initially elutes from the column with minimal changes in the composition regarding the reference flow, and the total elimination of water from the stream is never achieved. The concentration of water on stream decays up to reaching a constant value. The conclusions obtained from Fig. 6d are comparable with those previously described from the kinetic assays in static conditions (Fig. 5). In fact, water adsorption in dynamic conditions is also faster on microporous samples (i.e., O-XG and S-XG), adsorption rate being also favoured by highly hydrophilic oxygenated surface groups. In the case of N-XG, water adsorption was higher but also slower due to larger diffusion limitations. After stabilization, the lowest water adsorption, i.e., the highest  $C/C_0$  values at the column exit, corresponds to C-XG, which is also in agreement with the long period needed to saturate, even under static conditions at 100 % RH.

When comparing water and ethylene adsorption processes, a slope change in the water adsorption curve occurs at  $t_{0.02}$  in the undoped C-XG sample (Fig. 7a), while sulphur-doping leads to a slight delay in the water adsorption regarding  $t_{0.02}$  (Fig. 7c), this effect being more evident for O-XG (Fig. 7b) and mainly for N-XG (Fig. 7d), where water concentration stabilizes only after  $t_{0.90}$  for ethylene adsorption. Regarding dry conditions, humidity has a deeper influence on the shift to lower times on stream on the breakthrough point ( $X_{0.02}$ ) than on the saturation point ( $X_{0.90}$ ), thus favouring the separation between both characteristic points. This fact is clearly denoted by the smaller slopes of the adsorption curves compared to those obtained in dry conditions (Fig. 6a vs. b). Adsorbed water molecules reduce the ethylene accessibility and diffusion inside the pores, in such a manner that a greater proportion of ethylene is forced to remain in the gas flux, being identified at the column exit (breakthrough point,  $X_{0.02}$ ) at shorter times. Similarly, saturation ( $X_{0.90}$ ) is also reached earlier because of the lower porosity available.

The profiles of the ethylene breakthrough curves depend on the adsorbate–adsorbent interactions, determined by the extent of the mass transference zone (MTZ) and the gradient of concentration along this fraction of the column. The parameters  $H_{\text{MTZ}}$  and  $R_{\text{MTZ}}$  were calculated for all materials in both humid and dry conditions, and results are compiled in Table 6. Both parameters,  $H_{\text{MTZ}}$  and  $R_{\text{MTZ}}$ , are directly related with the nature and strength of interactions between adsorbate–adsorbent. A larger MTZ moving faster is evidently related with a weaker ethylene-adsorbent interaction.

In dry conditions, the smallest  $H_{\text{MTZ}}$  and  $R_{\text{MTZ}}$  values were obtained for the undoped C-XG, and then they remained practically unchanged after sulphur-doping (S-XG), but progressively increased for N-XG and specially, for O-XG. This tendency, i.e.,  $C \approx S < N < O$ , is clearly related with the Pauling's electronegativity (EN) of the corresponding

heteroatom introduced in the carbon support and its surface chemistry, i.e., C (2.55), S (2.58), N (3.04) and O (3.44), respectively. In this context, the higher EN of heteroatoms induces a progressive variation of the polar character of the surface groups and consequently, a smaller interaction with ethylene, increasing  $H_{\text{MTZ}}$  and  $R_{\text{MTZ}}$  values. In fact, a linear relationship between EN and  $H_{\text{MTZ}}$  or  $R_{\text{MTZ}}$  values was plotted in Fig. 8. Under humid conditions, both  $H_{\text{MTZ}}$  and  $R_{\text{MTZ}}$  values increased in all samples regarding dry conditions, denoting a weaker interaction of the available sites on surface with the ethylene molecules. The smaller influence of samples' surface chemistry on the column performance in humid conditions is also pointed out by the smaller slope of the linear fitting  $R_{\text{MTZ}}$  vs. EN (Fig. 8b). Although the variation of both parameters follows a similar tendency to dry conditions ( $C \approx S < N < O$ ), for low polar surfaces (e.g., C-XG and S-XG)  $H_{\text{MTZ}}$  values only increased moderately after water adsorption, while a strong increase of this parameter is observed for O-XG and N-XG. On the contrary, the increase of the  $R_{\text{MTZ}}$  values is deeper on C-XG and S-XG samples (Table 6 and Fig. 8a).

All these changes induced by water adsorption are in agreement with the previously commented adsorption mechanism [51,52]. In carbon xerogels, where initially high polar and hydrophilic N and O-sites are already present, the surface groups quickly interact with the moisture (Fig. 5d and Fig. 6d). This fact is also favoured because O- and N-surface groups are located preferentially on the external surface, as opposed to S-ones, as previously denoted by XPS analysis. Adsorbed water quickly blocks a fraction of the external porosity, which hinders the accessibility of ethylene, increasing the  $H_{\text{MTZ}}$ , but once inside the adsorbent particle,  $R_{\text{MTZ}}$  is close to the values obtained in dry conditions. Water adsorption only forms water clusters, the diffusion inside the pores is still governed by diffusion in gas phase and water is adsorbed preferentially on hydrophilic surface sites, while ethylene occupies the hydrophobic fraction of the surface, and thereby, adsorption is not competitive. This finding is also in agreement with the profiles of the adsorption curves. When water adsorption is energetically favourable regarding the ethylene one, which should occur mainly on doped carbon xerogels, water should displace the previously adsorbed ethylene, and typically  $C/C_0 > 1$  before reaching again the saturation ( $C/C_0 = 1$ ). However, ethylene desorption is not observed in any case either. Thus, both adsorbates are not in competition by the same sites under these experimental conditions.

In C-XG and S-XG samples, where water adsorption on the external surface is limited by the absence of hydrophilic groups, the accessibility into the porosity does not change significantly ( $H_{\text{MTZ}}$  changes moderately), ethylene and water vapour filling progressively and simultaneously the microporosity (both observed at the same time at  $\sim t_{0.02}$ ). Because of this simultaneous filling, the polarity of the surface deeply increased with water adsorption, the interaction with ethylene decreased and consequently,  $R_{\text{MTZ}}$  increased. In these samples, the microporosity of the adsorbent comprising the MTZ is simultaneously filled by both adsorbates,  $t_{0.02}$  being coincident with the stabilization of water concentration, which continues filling larger pores during a long time, as demonstrated in static conditions. In this porosity range, however, ethylene adsorption is limited and saturation is reached after some minutes. In O-XG and N-XG, the stronger interaction between water vapour and surface sites inside porosity, which are homogeneously distributed in the bulk, retards the movement of water regarding ethylene. Thus, in both cases, water concentration at  $t_{0.02}$  still decays more significantly in the case of N-XG because of the highest diffusional restriction imposed by its porosity. Finally, in this sample, water concentration only stabilized after the adsorbent is saturated with ethylene, but even so, the ethylene adsorbed is not removed by water.

Another important aspect to consider is the potential of the saturated samples to be regenerated and reused under the same conditions. For this purpose, the reference C-XG material and the N-doped sample (N-XG) were selected to perform three consecutive adsorption/desorption cycles under dry and humid conditions (Fig. 9). These samples were selected since they were the ones that showed the lowest and highest amount of water adsorbed under dynamic conditions, respectively. The

**Table 6**

$H_{\text{MTZ}}$  and  $R_{\text{MTZ}}$  obtained from ethylene breakthrough curves for the carbon xerogels.

Sample	$H_{\text{MTZ}}$ dry (cm)	$R_{\text{MTZ}}$ dry (cm/h)	$H_{\text{MTZ}}$ humid (cm)	$R_{\text{MTZ}}$ humid (cm/h)
C-XG	1.26	3.15	1.88	4.82
O-XG	2.40	5.78	4.55	6.12
S-XG	1.32	3.15	2.06	5.09
N-XG	1.73	5.08	3.40	5.78

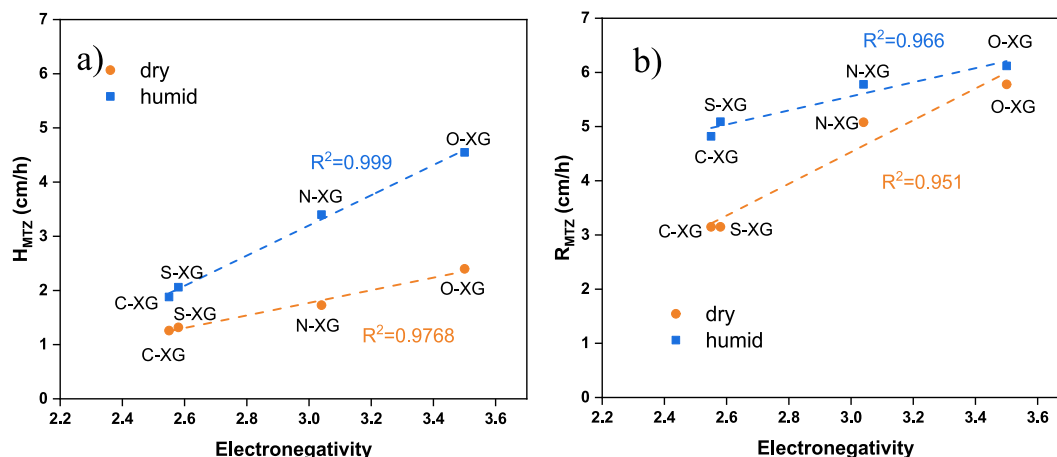


Fig. 8. Relationship between Pauling's electronegativity of the heteroatom-doping and a)  $H_{MTZ}$  and b)  $R_{MTZ}$  values obtained under dry and humid conditions in dynamic assays.

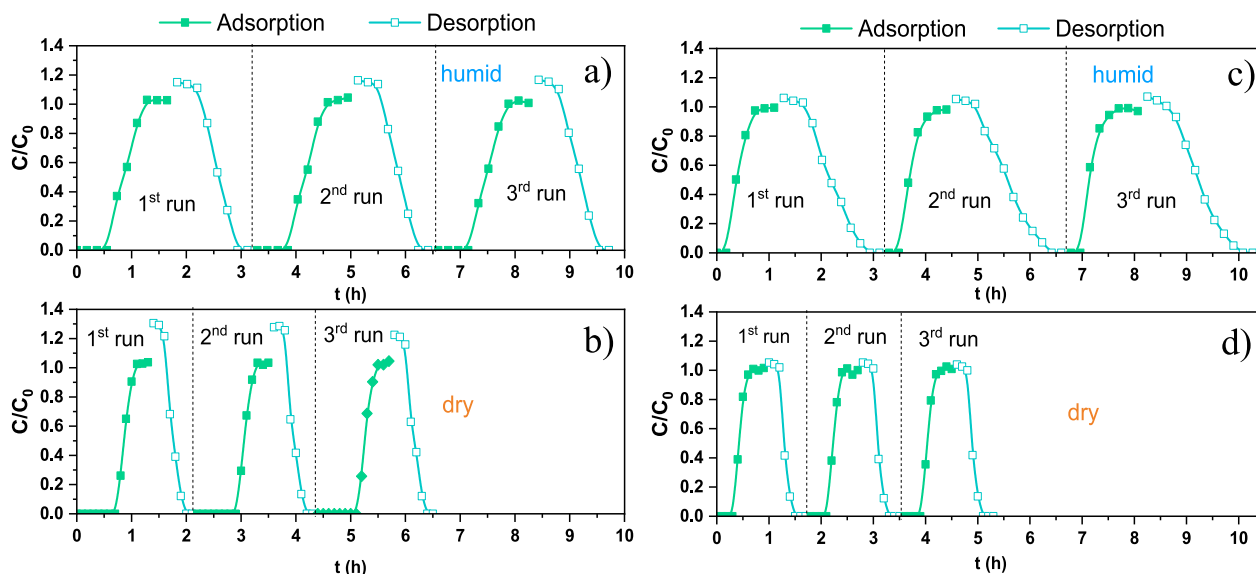


Fig. 9. Consecutive adsorption–desorption cycles in dynamic assays for (a, b) C-XG and (c, d) N-XG under (a, c) humid and (b, d) dry conditions.

desorption experiments were performed by exchanging the air/ $C_2H_4$  flow by a similar total flow of pure air, maintaining the column at room temperature. As observed in Fig. 9, the selected carbon xerogels were completely regenerated at room temperature regardless of RH%, porosity or surface chemistry of the samples. The adsorption–desorption profiles are maintained after three consecutive adsorption–desorption cycles, showing a complete reversibility of the processes, and also the reproducibility of the data previously obtained. No chemical or structural changes occurred, so the adsorptive behaviour was maintained, which means that the materials were stable under the conditions used. On the other hand, cycles are also almost symmetrical, indicating similar adsorption and desorption rates, although a major ethylene concentration is observed at the beginning of regeneration, leading to  $C/C_0$  values slightly higher than that. Nevertheless, some differences can be noticed depending on the presence of N-doping and moisture, both factors retarding the adsorption–desorption processes of ethylene, as previously commented, so longer cycles are required in this sense. The slope of the adsorption curves (adsorption rate) is also higher for C-XG in dry conditions. The slower adsorption–desorption processes, and consequently, the longer regeneration cycles, are detected accordingly for N-XG in humid conditions.

There are not many references in the literature concerning the adsorption of ethylene on carbon materials and most of them deal with static tests (determining the adsorption isotherm), being even scarcer those carried out under dynamic conditions and considering the effect of humidity. Nevertheless, the conclusions reached in this work on the influence of the physicochemical characteristics of the samples on the ethylene adsorption process are clearly in line with previous results. For instance, Wang *et al.* developed activated carbon fibers from cellulosic biomass by reductive oxidation to reduce the O-content, and thus, hydrophilic groups. They concluded that by diminishing these polar groups, the ethylene adsorption was enhanced [53]. Li *et al.* reached the same conclusion by modifying the surface chemistry of commercial coal-based activated carbons (ACs) with N groups. They studied the effect of hydrophilicity and relative humidity on toluene adsorption, another non-polar VOC, like ethylene. Their results also confirmed that the presence of polar groups in the carbon material and the increase of relative humidity hinder the adsorption of non-polar VOCs [55]. In a previous manuscript [39], we determined the ethylene adsorption capacity of both commercial ACs and home-made ACs prepared from agro-food industry wastes (olive stones) by chemical and physical procedures, using the same dynamic adsorption system, but using ethylene

concentrations between 250 – 1000 ppm and only under dry conditions. The reported results are also in agreement with those previously discussed about the influence of the narrow microporosity on the ethylene adsorption capacity. However, the adsorption capacity of these carbon xerogels is clearly smaller than that obtained with ACs from olive stones (e.g., these ACs presented the best performance of undoped materials in the literature), the different experimental conditions used are noteworthy, as well as the different physicochemical properties of each series of samples, optimized in each study for different objectives. In fact, the ethylene adsorption capacity was optimized through the control of the pore size distribution of ACs by activations, while these new doped carbon xerogels were prepared to assess the influence of different heteroatom-containing groups on ethylene adsorption capacity.

#### 4. Conclusions

Heteroatom-doped (O, N, S) carbon xerogels were synthesized by fitting the polymerization of resorcinol with different heterocyclic aldehydes. The sol–gel process, and consequently, parameters such as the primary particle size and overlapping degree, change according to the aldehyde used, thus doping influences simultaneously on both porosity and surface chemistry. Heteroatom-doped carbon xerogels displayed a hierarchical porosity with a micro-mesoporous character and BET surface areas ranging between 450–550 m<sup>2</sup>/g. The oxygen functionalities increased regarding the reference material (C-XG) in all doped samples, and significant contents of S- or N-surface groups were achieved on S-XG and N-XG, respectively. All these changes influence on the surface hydrophilicity. Water adsorption experiments carried out under static conditions pointed out that the volume of water adsorbed is in good agreement with the total porosity volume determined by N<sub>2</sub>-adsorption. Chemical functionalities allow to improve the water adsorption capacity of samples compared to those reported in literature [52]. Ethylene adsorption was performed under dynamic conditions in both dry and humid conditions, doping and moisture leading to a negative effect on its adsorption. The microporosity of the samples governed the adsorption capacity, while the efficiency of the column was influenced by the nature and strength of ethylene-adsorbent interactions. Thus, an increased electronegativity of the doping element resulted in larger and faster mass transfer zones. Ethylene and water adsorption were found to be non-competitive. The ethylene adsorption on these samples is completely reversible regardless of the presence of moisture in the flow or the physicochemical properties of adsorbents, although adsorption/desorption kinetics were slower in doped samples or humid conditions.

In future work, carbon xerogels should be activated to develop the microporosity and thereby, adsorption capacity, but as demonstrated, heteroatoms exert a negative effect on the adsorption of non-polar VOCs, which may help in the selection of appropriate raw materials, and in the adaption of synthesis procedures for specific adsorbents.

#### CRedit authorship contribution statement

**Lorena T. Pérez-Poyatos:** Writing – original draft, Methodology, Investigation, Formal analysis. **Sergio Morales-Torres:** Writing – review & editing, Supervision, Methodology, Data curation, Conceptualization. **Luisa M. Pastrana-Martínez:** Writing – review & editing, Supervision, Formal analysis, Data curation, Conceptualization. **Francisco J. Maldonado-Hódar:** Writing – review & editing, Validation, Supervision, Resources, Project administration, Funding acquisition, Conceptualization.

#### Declaration of competing interest

The authors declare that they have no known competing financial interests or personal relationships that could have appeared to influence the work reported in this paper.

#### Data availability

Data will be made available on request.

#### Acknowledgements

This work was financially supported by projects with ref. PCI2020-112045 funded by MICIU/AEI/10.13039/501100011033 and “European Union Next Generation EU/PRTR”, as part of the PRIMA Programme (Nano4Fresh project), ref. PID2021-126579OB-C31 by MICIU/AEI/10.13039/501100011033 and “ERDF A way of making Europe”, and by Junta de Andalucía - Conserjería de Universidad, Investigación e Innovación - Project P21\_00208. L.T.P.-P. (FPU22/01255) and S.M.-T. (RYC-2019-026634-I) are grateful to MICIN/AEI/10.13039/501100011033 and FSE “El FSE invierte en tu futuro” for their FPU predoctoral and Ramon y Cajal research contracts, respectively. “Unidad de Excelencia Química Aplicada a Biomedicina y Medioambiente” of the University of Granada (UEQ-UGR) is gratefully acknowledged for the technical assistance. Funding for open access charge: Universidad de Granada / CBUA.

#### Appendix A. Supplementary data

Supplementary data to this article can be found online at <https://doi.org/10.1016/j.jcis.2024.08.044>.

#### References

- [1] K. Tripathi, S. Pandey, M. Malik, T. Kaul, Fruit ripening of climacteric and non climacteric fruit, *J. Environ. Appl. Biores.* 4 (2016) 27–34.
- [2] P. Tepamatr, Efficacy of a palladium-modified activated carbon in improving ethylene removal to delay the ripening of gros michel banana, *J. Agric. Food Res.* 12 (2023) 100561.
- [3] N. Pathak, O.J. Caleb, C. Rauh, P.V. Mahajan, Efficacy of photocatalysis and photolysis systems for the removal of ethylene under different storage conditions, *Postharvest Biol. Technol.* 147 (2019) 68–77.
- [4] C. Dias, T. Ribeiro, A.C. Rodrigues, A. Ferrante, M.W. Vasconcelos, M. Pintado, Improving the ripening process after 1-MCP application: implications and strategies, *Trends Food Sci. Technol.* 113 (2021) 382–396.
- [5] A. Ebrahimi, M. Zabihzadeh Khajavi, A.M. Mortazavian, H. Asilian-Mahabadi, S. Rafiee, M. Farhoodi, S. Ahmadi, Preparation of novel nano-based films impregnated by potassium permanganate as ethylene scavengers: an optimization study, *Polym. Test.* 93 (2021) 106934.
- [6] L. Cisneros, F. Gao, A. Corra, Silver nanocluster in zeolites. Adsorption of ethylene traces for fruit preservation, *Microporous Mesoporous Mater.* 283 (2019) 25–30.
- [7] S.D. do Nascimento Sousa, R.G. Santiago, D.A. Soares Maia, E. de Oliveira Silva, R. S. Vieira, M. Bastos-Neto, Ethylene adsorption on chitosan/zeolite composite films for packaging applications, *Food Packag. Shelf Life* 26 (2020) 100584.
- [8] W. Liang, Y. Zhang, X. Wang, Y. Wu, X. Zhou, J. Xiao, Y. Li, H. Wang, Z. Li, Asphalt-derived high surface area activated porous carbons for the effective adsorption separation of ethane and ethylene, *Chem. Eng. Sci.* 162 (2017) 192–202.
- [9] S.-H. Wang, Y.-K. Hwang, S.W. Choi, X. Yuan, K.B. Lee, F.-C. Chang, Developing self-activated lignosulfonate-based porous carbon material for ethylene adsorption, *J. Taiwan Inst. Chem. Eng.* 115 (2020) 315–320.
- [10] M.H. Álvarez-Hernández, F. Artés-Hernández, F. Ávalos-Belmontes, M.A. Castillo-Campohermoso, J.C. Contreras-Esquivel, J.M. Ventura-Sobrevilla, G.B. Martínez-Hernández, Current scenario of adsorbent materials used in ethylene scavenging systems to extend fruit and vegetable postharvest life, *Food Bioprocess Technol.* 11 (3) (2018) 511–525.
- [11] S. Morales-Torres, F.J. Maldonado-Hódar, A.F. Pérez-Cadenas, F. Carrasco-Marín, Structural characterization of carbon xerogels: from film to monolith, *Microporous Mesoporous Mater.* 153 (2012) 24–29.
- [12] R.W. Pekala, Organic aerogels from the polycondensation of resorcinol with formaldehyde, *J. Mater. Sci.* 24 (9) (1989) 3221–3227.
- [13] I.E. Men'shchikov, A.V. Shkolin, E.V. Khozina, A.E. Grinchenko, A.A. Fomkin, Mesoporous carbon xerogel as a promising adsorbent for capture and storage of liquefied natural gas vapors, *Adsorption* 29 (5) (2023) 255–273.
- [14] G.C. Ruben, R.W. Pekala, High-resolution transmission electron microscopy of the nanostructure of melamine-formaldehyde aerogels, *J. Non-Cryst. Solids* 186 (1995) 219–231.
- [15] L. Wang, X. Hu, R. Huang, M. Huang, X. Liu, Z. Zhou, P. Guo, Z. Mao, X. Xu, X. Wang, Elastic, antifracking phenolic aerogels for advanced thermal protection at extreme environments, *Compos. Commun.* 48 (2024) 101889.
- [16] Y. Lee, J.S. Yoon, D.J. Suh, C.-H. Lee, Y.-W. Suh, 5-hydroxymethylfurfural as a potential monomer for the preparation of carbon aerogel, *Mater. Chem. Phys.* 136 (2) (2012) 837–844.

- [17] H. Jirglová, A.F. Pérez-Cadenas, F.J. Maldonado-Hódar, Synthesis and properties of phloroglucinol–phenol–formaldehyde carbon aerogels and xerogels, *Langmuir* 25 (4) (2009) 2461–2466.
- [18] Á. Sánchez-Sánchez, F. Suárez-García, A. Martínez-Alonso, J.M.D. Tascón, Synthesis, characterization and dye removal capacities of N-doped mesoporous carbons, *J. Colloid Interface Sci.* 450 (2015) 91–100.
- [19] K.Y. Kang, B.I. Lee, J.S. Lee, Hydrogen adsorption on nitrogen-doped carbon xerogels, *Carbon* 47 (4) (2009) 1171–1180.
- [20] H. Cui, J. Xu, J. Shi, C. Zhang, Synthesis of sulfur doped carbon from dipotassium anthraquinone-1,8-disulfonate for CO<sub>2</sub> adsorption, *J. CO<sub>2</sub> Util.* 50 (2021) 101582.
- [21] Y. Gao, Q. Wang, G. Ji, A. Li, J. Niu, Doping strategy, properties and application of heteroatom-doped ordered mesoporous carbon, *RSC Adv.* 11 (10) (2021) 5361–5383.
- [22] F.J. Maldonado-Hódar, C. Moreno-Castilla, F. Carrasco-Marín, A.F. Pérez-Cadenas, Reversible toluene adsorption on monolithic carbon aerogels, *J. Hazard. Mater.* 148 (3) (2007) 548–552.
- [23] J.F. Vivo-Vilches, F. Carrasco-Marín, A.F. Pérez-Cadenas, F.J. Maldonado-Hódar, Fitting the porosity of carbon xerogel by CO<sub>2</sub> activation to improve the TMP/n-octane separation, *Microporous Mesoporous Mater.* 209 (2015) 10–17.
- [24] X. Dai, Y. Wang, X. Wang, S. Tong, X. Xie, Polarity on adsorption and photocatalytic performances of N-GR/TiO<sub>2</sub> towards gaseous acetaldehyde and ethylene, *Appl. Surf. Sci.* 485 (2019) 255–265.
- [25] N. Job, A. Théry, R. Pirard, J. Marien, L. Kocon, J.-N. Rouzaud, F. Béguin, J.-P. Pirard, Carbon aerogels, cryogels and xerogels: Influence of the drying method on the textural properties of porous carbon materials, *Carbon* 43 (12) (2005) 2481–2494.
- [26] E. Gallegos-Suárez, A.F. Pérez-Cadenas, F.J. Maldonado-Hódar, F. Carrasco-Marín, On the micro- and mesoporosity of carbon aerogels and xerogels. The role of the drying conditions during the synthesis processes, *Chem. Eng. J.* 181–182 (2012) 851–855.
- [27] C. Lin, J.A. Ritter, Carbonization and activation of sol–gel derived carbon xerogels, *Carbon* 38 (6) (2000) 849–861.
- [28] C. Leon, L. Radovic, Chemistry and physics of carbon, Thrower, Marcel Dekker, New York, 1994.
- [29] L.M. Pastrana-Martínez, S. Morales-Torres, V. Likodimos, P. Falaras, J. L. Figueiredo, J.L. Faria, A.M.T. Silva, Role of oxygen functionalities on the synthesis of photocatalytically active graphene–TiO<sub>2</sub> composites, *Appl Catal B* 158–159 (2014) 329–340.
- [30] H.P. Boehm, Chemical identification of surface groups, in: D.D. Eley, H. Pines, P. B. Weisz (Eds.), *Adv. Academic Press, Catal.*, 1966, pp. 179–274.
- [31] S. Brunauer, P.H. Emmett, E. Teller, Adsorption of gases in multimolecular layers, *J. Am. Chem. Soc.* 60 (2) (1938) 309–319.
- [32] R.C. Bansal, J.-B. Donnet, F. Stoeckli, Active carbon, M. Dekker, New York, 1988.
- [33] F. Rouquerol, J. Rouquerol, K. Sing, Adsorption by powders and porous solids, Methodology and Applications, Academic Press, London, Principles, 1999, pp. 219–228.
- [34] F. Stoeckli, Porosity in carbons, Characterization and applications, Arnold, London, 1995.
- [35] T.L.S. Silva, S. Morales-Torres, J.L. Figueiredo, A.M.T. Silva, Multi-walled carbon nanotube/PVDF blended membranes with sponge- and finger-like pores for direct contact membrane distillation, *Desalination* 357 (2015) 233–245.
- [36] E.P. Barrett, L.G. Joyner, P.P. Halenda, The determination of pore volume and area distributions in porous substances. I. Computations from nitrogen isotherms, *J. Am. Chem. Soc.* 73 (1) (1951) 373–380.
- [37] P.I. Ravikovitch, G.L. Haller, A.V. Neimark, Density functional theory model for calculating pore size distributions: pore structure of nanoporous catalysts, *Adv. Colloid Interface Sci.* 76–77 (1998) 203–226.
- [38] A.V. Neimark, Y. Lin, P.I. Ravikovitch, M. Thommes, Quenched solid density functional theory and pore size analysis of micro-mesoporous carbons, *Carbon* 47 (7) (2009) 1617–1628.
- [39] A.M. Regadera-Macías, S. Morales-Torres, L.M. Pastrana-Martínez, F.J. Maldonado-Hódar, Optimizing filters of activated carbons obtained from biomass residues for ethylene removal in agro-food industry devices, *Environ. Res.* 248 (2024) 118247.
- [40] A.M. Regadera-Macías, S. Morales-Torres, L.M. Pastrana-Martínez, F.J. Maldonado-Hódar, Ethylene removal by adsorption and photocatalytic oxidation using biocarbon–TiO<sub>2</sub> nanocomposites, *Catal. Today* 413–415 (2023) 113932.
- [41] C. Mahendra, P.M. Sathya Sai, C. Anand Babu, K. Revathy, K.K. Rajan, Analysis and modeling of fixed bed sorption of cesium by AMP-PAN, *J. Environ. Chem. Eng.* 3 (3) (2015) 1546–1554.
- [42] R.W. Pekala, C.T. Alviso, J.D. LeMay, Organic aerogels: microstructural dependence of mechanical properties in compression, *J. Non-Cryst. Solids* 125 (1) (1990) 67–75.
- [43] K.S.W. Sing, Reporting physisorption data for gas/solid systems with special reference to the determination of surface area and porosity, *Pure Appl. Chem.* 57 (4) (1985) 603–619.
- [44] W. Kiciński, A. Dziura, Heteroatom-doped carbon gels from phenols and heterocyclic aldehydes: sulfur-doped carbon xerogels, *Carbon* 75 (2014) 56–67.
- [45] W. Kiciński, M. Norek, A. Dziura, M. Polański, Copolycondensation of heterocyclic aldehydes: a general approach to sulfur and nitrogen dually-doped carbon gels, *Microporous Mesoporous Mater.* 225 (2016) 198–209.
- [46] W. Kiciński, M. Norek, B.J. Jankiewicz, Heterogeneous carbon gels: N-doped carbon xerogels from resorcinol and N-containing heterocyclic aldehydes, *Langmuir* 30 (47) (2014) 14276–14285.
- [47] N. de la Torre-Miranda, L. Reilly, P. Eloy, C. Poleunis, S. Hermans, Thiol functionalized activated carbon for gold thiosulfate recovery, an analysis of the interactions between gold and sulfur functions, *Carbon* 204 (2023) 254–267.
- [48] A. Misra, P.K. Tyagi, M.K. Singh, D.S. Misra, FTIR studies of nitrogen doped carbon nanotubes, *Diamond Relat. Mater.* 15 (2) (2006) 385–388.
- [49] S.J. Shin, J.H. Jang, S.-H. Yoon, I. Mochida, A study on the effect of heat treatment on functional groups of pitch based activated carbon fiber using FTIR, *Carbon* 35 (1997) 1739–1743.
- [50] W. Kiciński, S. Dyjak, Nitrogen-doped carbons derived from imidazole-based cross-linked porous organic polymers, *Molecules* 26 (3) (2021) 668.
- [51] C. Zheng, H.K. Song, Y.C. Xie, X.L. Yang, L. Lan, K.L. Kang, S. Bai, Modeling of multi-temperature IV and V-type water vapor adsorption isotherms on activated carbons for chemical protection, *Colloids Surf. A: Physicochemical Engineering Aspects* 670 (2023) 131486.
- [52] M. Kéri, D. Nyul, K. László, L. Novák, I. Bányai, Interaction of resorcinol-formaldehyde carbon aerogels with water: a comprehensive NMR study, *Carbon* 189 (2022) 57–70.
- [53] Y.-H. Wang, S. Bayatpour, X. Qian, B. Frigo-Vaz, P. Wang, Activated carbon fibers via reductive carbonization of cellulosic biomass for adsorption of nonpolar volatile organic compounds, *Colloids Surf., A* 612 (2021) 125908.
- [54] Z.E. Lim, Q.B. Thai, D.K. Le, T.P. Luu, P.T.T. Nguyen, N.H.N. Do, P.K. Le, N. Phan-Thien, X.Y. Goh, H.M. Duong, Functionalized pineapple aerogels for ethylene gas adsorption and nickel (II) ion removal applications, *J. Environ. Chem. Eng.* 8 (6) (2020) 104524.
- [55] J. Li, X. Ma, H. Wu, L. Yang, Adsorption of low-concentration VOCs on modified activated carbons in a humid atmosphere, *Energy Fuels* 35 (6) (2021) 5090–5100.